Experimental Demonstration of the Oscillatory Snake Instability of the Bright Soliton of the (2 + 1)D Hyperbolic Nonlinear Schrödinger Equation

S.-P. Gorza,[1] B. Deconinck,[2] Ph. Emplit,[1] T. Trogdon,[2] and M. Haelterman[1]

[1]*Service OPERA-photonique, Université libre de Bruxelles (ULB), 50 Avenue F. D. Roosevelt, CP194/5 B-1050 Bruxelles, Belgium*
[2]*Department of Applied Mathematics, University of Washington Campus Box 352420, Seattle, Washington, 98195, USA.*

(Received 3 December 2010; published 1 March 2011)

The transition between the standard snake instability of bright solitons of the hyperbolic nonlinear Schrödinger equation and the recently theoretically predicted oscillatory snake instability is experimentally demonstrated. The existence of this transition is proven on the basis of spatiotemporal spectral features of bright soliton laser beams propagating in normally dispersive Kerr-type nonlinear planar waveguides.

DOI: 10.1103/PhysRevLett.106.094101 PACS numbers: 05.45.Yv, 42.65.Sf, 42.65.Tg, 42.65.Wi

Since its appearance in the field of hydrodynamics, the concept of soliton has steadily and deeply penetrated into most branches of physics. This growing success is the result of both the fundamental interest and the potential applications of solitons. In many physical contexts, solitons are theoretically described as solutions of a nonlinear wave equation with a number of transverse dimensions that is reduced with respect to the actual dimensionality of the system in which they evolve. This is, for instance, the case for deep-water surface wave solitons and spatial optical solitons propagating in dispersive media. However these low-dimensional solitons, also called soliton stripe, were shown to be unstable against periodic perturbations in the extra transverse dimensions in which they are uniform, regardless of the relative sign between the dispersion (diffraction) terms, i.e., both in elliptic and hyperbolic systems [1,2]. In hyperbolic systems, standard perturbation theory has shown that bright soliton stripes are unstable against snakelike deformations, and this was experimentally confirmed both in optics [3] and in hydrodynamics [4]. However, recent studies have revealed a certain degree of complexity in hyperbolic systems by showing unexpectedly that the bright soliton stripe is also unstable against necklike deformations [5,6]. Neck and snake instabilities have also been reported in the discrete hyperbolic nonlinear Schrödinger (NLS) equation, which brings to light the universality of the instability mechanisms induced by extra dimensions in nonlinear systems [7]. Besides their fundamental interest, the understanding of these transverse instabilities is crucial in practice, as they constitute obstacles to practical applications of optical solitons. In this regard, several studies have shown that additional physical phenomena naturally present in practical nonlinear systems can eliminate transverse instabilities [8–10].

In the present Letter, we report on an experimental study, in the context of optics, of the transverse instability of the one-dimensional (1D) bright soliton solution of the (2 + 1)D hyperbolic nonlinear Schrödinger equation, in the short wavelength perturbation regime. From a theoretical point of view, this problem was proved to be rather delicate and even controversial (see the review reported in [11]). Indeed, the snake instability gain spectrum was initially expected to exhibit a cutoff in the short wavelength perturbation regime [2], but numerical studies suggested that this expectation was ill-founded [12,13]. In a theoretical paper Deconinck *et al.* then showed that the snake instability cutoff is the appearance threshold of a new type of instability called "oscillatory snake instability." The cutoff has thus become a transition point where the snake instability growth rate starts to be complex, in agreement with the work of Anderson *et al.* [13]. These two instabilities give rise to the growth of a spatiotemporal zigzag deformation of the soliton stripe [see Figs. 1(b) and 1(c)]. However, the imaginary part of the instability growth rate manifests itself by a drift of the spatiotemporal undulation in the comoving time frame traveling at the group velocity of the stripe. The object of our work is to demonstrate the absence of a definite instability cutoff and to confirm in this way the scenario of the transition between the standard and the oscillatory snake instabilities.

Let us consider the hyperbolic NLS equation with two transverse dimensions. In dimensionless variables it reads

$$i\frac{\partial\psi}{\partial\zeta}+\frac{1}{2}\frac{\partial^2\psi}{\partial\xi^2}-\frac{1}{2}\frac{\partial^2\psi}{\partial\tau^2}+|\psi|^2\psi=0. \qquad (1)$$

In hydrodynamics, this equation describes the evolution of the elevation of the water wave surface for slowly modulated wave trains in deep water. In optics, the same equation governs the propagation of electromagnetic fields in self-focusing and normally dispersive planar waveguides. The slowly varying spatiotemporal envelope of the electric field is then $E = A_0\psi$, while the propagation coordinate is $z = \zeta L_{\mathrm{NL}}$, the transverse (in-plane) coordinate is $x = \xi(L_{\mathrm{NL}}/k_0)^{1/2}$ and $t = \tau(L_{\mathrm{NL}}k_0'')^{1/2}$ is the time in the comoving reference frame traveling at the group velocity of light. In these expressions, $L_{\mathrm{NL}} = 1/(\gamma A_0^2)$ is the nonlinear length, where γ is the nonlinear coefficient of

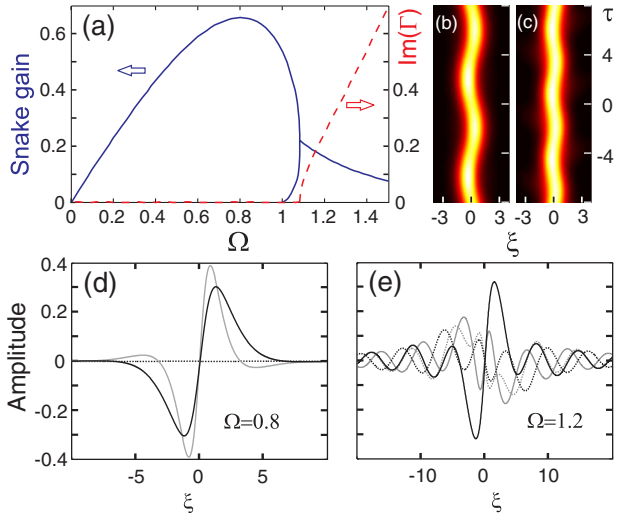

FIG. 1 (color online). (a) Snake instability gain $g = 2\mathrm{Re}(\Gamma)$ [solid (blue) line] and imaginary part of Γ [dashed (red) line] plotted as a function of the perturbation frequency Ω. Beyond the frequency cutoff $\Omega_c \approx 1.08$, Γ is complex and the snake instability becomes oscillatory. (b),(c) Density plot of the spatiotemporal intensity profile for $\epsilon_0 = 1$ and $\Omega = 0.8$ and 1.2, respectively. (d),(e) Eigenfunctions U (gray) and V (black) plotted as a function of the transverse coordinate ξ below (b) and above (c) Ω_c. Solid lines stand for the real part and dashed lines for the imaginary part. Figures adapted from [5].

the waveguide; k_0 is the guided-mode propagation constant and k_0'' is the group velocity dispersion coefficient.

The bright soliton stripe solution of Eq. (1) is $\psi = \mathrm{sech}(\xi)\exp(i\zeta/2)$. The stability analysis with respect to transverse perturbations [2,5] has shown that this solution is unstable against periodic perturbations of the form $p_\Gamma(\zeta, \xi, \tau) = \epsilon_0(u + iv)\exp(i\zeta/2)$ with $\{u, v\} = [\{U(\xi), V(\xi)\}\exp(i\Omega\tau + \Gamma\zeta) + c.c.]$, where the eigenfunctions $\{U, V\}$ are complex functions of the transverse coordinate ξ; Ω is the modulation frequency and $c.c$ denotes the complex conjugate of the previous term. The instability gain is then given by $g = 2\mathrm{Re}(\Gamma)$ so that g can be interpreted as an amplitude gain in hydrodynamics, while in optics, g is a power gain. Note that if the perturbation p_Γ, given by (U, V, Γ, Ω) is unstable with the gain g then $p^*_{\Gamma^*}$ described by $(U^*, V^*, \Gamma^*, \Omega)$ is also unstable with the same gain but opposite drift velocity. In Fig. 1, the instability gain and the imaginary part of Γ are plotted for the snake instability, i.e., for antisymmetric eigenfunctions [5]. For small frequency modulations Ω, Γ is real and the functions $\{U, V\}$ are real valued [see for instance the plots of U and V for $\Omega = 0.8$ in Fig. 1]. This instability is nothing but the well-known snake instability reported in [2] and subsequent works (see, e.g., [11]). As can be seen in Fig. 1, the instability gain reaches its maximum value near $\Omega = 0.8$ before decreasing rapidly. At the point of infinite slope, the gain curve merges with another gain curve starting at unit frequency [5]. More importantly, an additional gain curve branches from the two other ones at this merging cutoff point $\Omega_c \approx 1.08$. Theory shows that above the threshold $\Omega_c \approx 1.08$ the eigenvalue Γ as well as the eigenfunctions U and V are complex [see U and V plotted for $\Omega = 1.2$ in Fig. 1]. Quite remarkably this oscillatory snake instability exhibits no high frequency cutoff, which is fundamentally different from the instability of the soliton stripes of the elliptic NLS equation where a finite cutoff has been demonstrated [14].

Our experiments were performed in the context of optics with laser beams propagating in planar waveguides. The soliton stripe consists of a spatially localized beam with a temporal duration in the picosecond range to ensure the growth of the transverse instability. Moreover, the instability is seeded by an ancillary beam to have access to the variation of the snake gain with the modulation frequency.

The laser source consists of a mode-locked fiber laser delivering 3.86 ps pulses at 1536 nm, amplified in an Er-doped fiber amplifier of short length to limit pulse distortion. At the output of the amplifier, the laser beam is shaped and coupled into the planar guiding structure with a width of 17 μm and a TE polarization. The ancillary beam is generated by sending part of the fiber laser output into an Er:Yb co-doped fiber amplifier. The nonlinearities experienced by the picosecond pulses during the amplification process are responsible for the generation of broadband pulses whose spectrum ranges from 1480 nm up to 1680 nm. These pulses are then spectrally filtered to end up with tunable 6 nm-wide pulses with nearly the same temporal duration as the soliton beam. Before being recombined and synchronized with the soliton beam, the resulting ancillary beam passes through a π-phase step plate to efficiently seed the snake instability. Its polarization is also set to be identical to the soliton beam. The ratio between the seed and the soliton peak power is of the order of 10^{-4} in the frequency range of interest. At the output of the waveguide, the beam is collected by a microscope objective and sent onto an imaging spectrometer to record the angularly resolved spectrum. This spectrum is filtered to select one of the two sidebands before being imaged onto an InGaAs camera or sent to a power meter.

The planar waveguides are made up of a 1.4 μm-thick layer of $Al_{0.18}Ga_{0.82}$ As surrounded by two $Al_{0.24}Ga_{0.76}$ As layers. At the soliton beam wavelength, the TE-mode exhibits a normal dispersion equal to $k_0'' = 1.04 \times 10^{-24}$ s^2/m and a focusing Kerr nonlinearity characterized by $\gamma = 2.8 \times 10^{-3}$ W^{-1}, while the mode wave number is $k_0 = 1.33 \times 10^7$ m^{-1}.

Experiments were performed with 4 and 5 mm-long waveguides. The coupled peak power is 1.3 kW resulting in a nonlinear length of $L_{\mathrm{NL}} = 516$ μm. In normalized units, the soliton beam initial condition is then well approximated by $\psi = \exp(-[\xi/2.3]^2)\mathrm{sech}(\tau/94)$. The input beam width is slightly larger than the fundamental soliton width to compensate for the losses. Moreover, the pulse

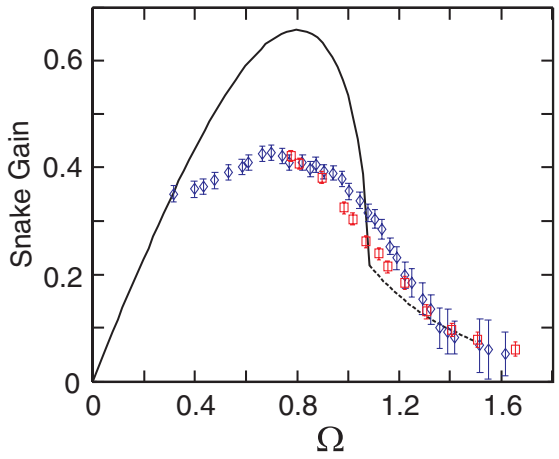

FIG. 2 (color online). Snake gain as a function of the normalized frequency perturbations Ω, experimentally recorded for two different slab waveguides [(blue) diamonds and (red) squares]. The solid and dashed lines show the theoretical snake and oscillatory snake gains, respectively.

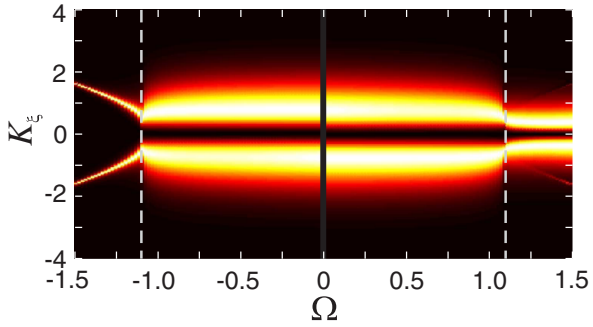

FIG. 3 (color online). Density plot of the theoretical evolution of the angularly resolved spectrum $|\tilde{p}_\Gamma|^2$ as a function of the frequency Ω. Each spatial spectra (i.e., each profiles for a given frequency Ω) has been normalized to unity. Brighter colors stand for larger amplitudes. The vertical dashed lines separate the snake ($|\Omega| < 1.08$) from the oscillatory snake ($|\Omega| > 1.08$) regimes.

duration $\Delta\tau = 166$ is around 1 order of magnitude larger than the modulation periods $2\pi/\Omega$ involved in our experiment [see Fig. 2]. As a consequence, the finite pulse duration does not significantly affect the dynamics of the instability.

The instability gain spectrum $\Gamma(\Omega)$ was first recorded to confirm the instability properties at low and high frequency modulations. This spectrum was obtained by measuring the output power in the seed sideband, with and without the soliton beam. As can be seen in Fig. 2, the normalized frequency detuning of the seed beam ranges between 0.3 and 1.65, allowing us to study the instability properties around the theoretical snake cutoff $\Omega_c \approx 1.08$. The measured instability gain is in good agreement with theory and clearly shows a maximum growth rate. However, the frequency at which the gain is maximum and the value of this gain are slightly lower than expected from theory. This is mainly due to the losses experienced in the waveguide but also to the finite time duration of the pulses and the pump depletion, as confirmed by numerical simulations. Nevertheless, the most important result that comes out is that no gain cutoff is observed for frequencies as high as $\Omega = 1.65$. Instead, the instability gain slowly decreases for shorter wavelength perturbations, as predicted by theory for the oscillatory snake instability gain spectrum. However, in Fig. 2 the discontinuity of the slope of the instability gain at the threshold of the oscillatory snake instability cannot be clearly identified. This is attributable to the spectral width of the picosecond pulses used in our experiment which, in normalized units, is of about 0.15. The experimentally recorded gain curve is therefore not sufficient to confirm unquestionably the existence of the transition between the snake instability and the oscillatory snake instability at the threshold frequency $\Omega_c \approx 1.08$. This situation thus calls for a finer characterization of the instability.

Beside the instability gain spectrum, a definite signature of the two instability regimes can be found in the angularly resolved spectrum of the unstable perturbation $|\tilde{p}_\Gamma(\omega, K_\xi)|^2 = |F\{p_\Gamma\}|^2$, where F denotes the two-dimensional Fourier-transform operation with respect to τ and ξ. The angularly resolved spectrum is made up of two peaks, $|\tilde{p}_\Gamma^-|^2$ and $|\tilde{p}_\Gamma^+|^2$, centered on $-\Omega$ and $+\Omega$, respectively. In Fig. 3, the two-dimensional spectrum $|\tilde{p}_\Gamma|^2$ has been plotted for frequency perturbations ranging from $\Omega = 0.02$ up to 1.5. In this figure, the two instability regimes can clearly be distinguished. For the snake instability, i.e., below the threshold Ω_c, the angularly resolved spectra in the two sidebands ($|\tilde{p}_\Gamma^+|^2$ and $|\tilde{p}_\Gamma^-|^2$) are identical and their shapes do not significantly evolve, except close to Ω_c. On the other hand, beyond the threshold, the spatial spectra are no longer the same in the two frequency sidebands. Moreover, a dramatic change occurs for $|\tilde{p}_\Gamma^-|^2$ since the two spectral peaks become narrower as Ω increases. These features allow us to better identify the two instabilities than a direct study of their dynamics in the spatio-temporal domain since the qualitative differences are more pronounced in the former domain [see Figs. 1(b) and 1(c)]. Note that the angularly resolved spectra of $\tilde{p}_{\Gamma^*}^*$ is the mirror image of $\tilde{p}_\Gamma$, centered on $\Omega = 0$. Beyond the threshold Ω_c we can therefore expect to experimentally observe the emergence of a four peaks structure resulting from the possible excitation of both p_Γ and $p_{\Gamma^*}^*$ [see Fig. 4].

The left and the right sides of Fig. 4(b) are the result of the compilation of the two-dimensional spectra of the two sidebands, experimentally recorded at the output of the waveguide for seed wavelengths between 1554 nm and 1604 nm by step of 2 nm. The left side of Fig. 4(b) shows the spectra recorded at the seed frequency (signal), while new frequencies generated by the instability growth correspond to the right side ($\Omega > 0$, idler). As can be seen, for

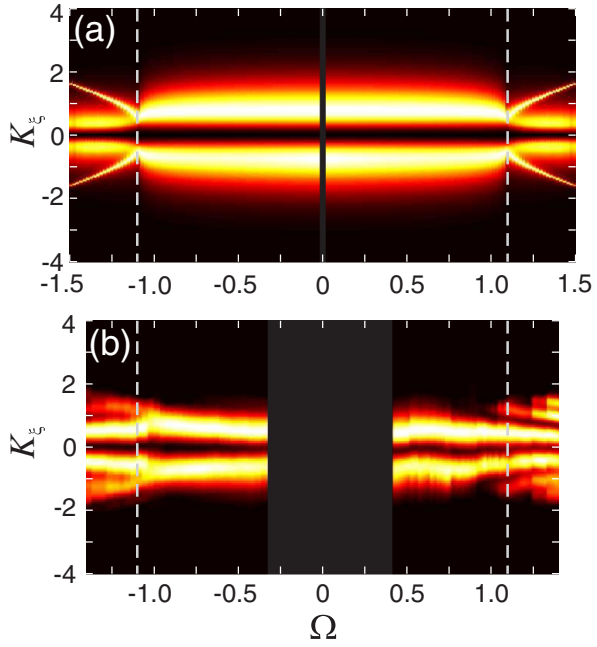

FIG. 4 (color online). (a) Same as for Fig. 3 but computed for $|\tilde{p}_\Gamma|^2 + |\tilde{p}^*_{\Gamma^*}|^2$. The vertical dashed line separates the snake ($|\Omega| < 1.08$) from the oscillatory snake ($|\Omega| > 1.08$) regimes. (b) Experimental results.

low frequency perturbations, the signal and the idler angular spectra show two separated broad peaks, which are characteristic of the snake instability. As the frequency increases beyond $\Omega = 1$, these two spectra start to be qualitatively different. On the signal side, the position of the main central peaks becomes closer to $K_\xi = 0$, as in Fig. 3 for $\Omega > 0$. At the same time, two new peaks appear in the spectrum and move away from the central lobes similarly to what can be seen in Fig. 3 but for $\Omega < 0$. The presence of four peaks on the signal and idler side can be understood by assuming that in our experiment, the initial condition seeds the two independent unstable modes $\tilde{p}_\Gamma$ and $\tilde{p}^*_{\Gamma^*}$ [see Fig. 4(a)]. Nevertheless, the asymmetry in the initial condition is reflected in the output spectra for frequencies above the threshold Ω_c [white dashed lines in Fig. 4]. This is particularly visible around $\Omega = 1.25$ where the outermost peaks are sharper and more intense in the idler sideband than in the signal sideband. These features constitute a genuine signature of the oscillatory snake instability. The appearance of extra peaks on the idler side for seed frequencies larger than $\Omega \approx 1.25$ can be explained by the growth of the oscillatory neck instability [5,6] whose spectrum is in good agreement with the position of these outermost peaks. Finally note that the experimental frequency threshold of the oscillatory snake instability is slightly lower than the theoretical threshold value Ω_c. This is attributable to the spectral width of the seed and soliton pulses as well as to the effect of losses. Along the propagation, losses lead indeed to a decrease of the frequency Ω_c expressed in real units.

In conclusion, by studying the angularly resolved spectra of a bright soliton laser beam propagating in a normally dispersive Kerr-type nonlinear planar waveguide, we demonstrated experimentally for the first time the existence of the oscillatory snake instability theoretically predicted for the hyperbolic NLS bright soliton. More precisely, we identified in the instability gain spectrum the threshold frequency corresponding to the transition between the standard snake instability and the oscillatory snake instability. The measured frequency threshold is in reasonably good agreement with theory of Ref. [5]. Our observations clearly confirm the practical relevance of this theory and clarify, in particular, the controversial issue of the unbounded instability spectrum. In view of the importance of hyperbolic NLS models in physical sciences, our work is liable to be of interest to other research fields such as, for instance, the field of hydrodynamics in which the formation of deep-water freak waves has been described as being driven by the well-known Benjamin-Feir instability of 3D uniform wave train solutions of the hyperbolic NLS equation [15].

This work was supported by the Belgian Science Policy Office under Grant No. IAP-VI10 and by the Fonds de la Recherche Fondamentale Collective, Grant No. 2.4513.06. S.-P. Gorza acknowledges the support of the Fonds de la Recherche Scientifique-FNRS.

[1] Y. S. Kivshar and D. E. Pelinovsky, Phys. Rep. **331**, 117 (2000).
[2] V. E. Zakharov and A. M. Rubenchik, Sov. Phys. JETP **38**, 494 (1974).
[3] S.-P. Gorza *et al.*, Phys. Rev. Lett. **92**, 084101 (2004).
[4] E. D. Brown *et al.*, J. Fluid Mech. **204**, 263 (1989).
[5] B. Deconinck, D. E. Pelinovsky, and J. D. Carter, Proc. R. Soc. A **462**, 2039 (2006).
[6] S.-P. Gorza *et al.*, Phys. Rev. Lett. **102**, 134101 (2009).
[7] A. V. Yulin, D. V. Skryabin, and A. G. Vladimirov, Opt. Express **14**, 12347 (2006).
[8] C. Anastassiou *et al.*, Phys. Rev. Lett. **85**, 4888 (2000).
[9] Y. Lin, R.-K. Lee, and Y. S. Kivshar, J. Opt. Soc. Am. B **25**, 576 (2008).
[10] Z. H. Musslimani and J. Yang, Opt. Lett. **26**, 1981 (2001).
[11] D. E. Pelinovsky, Math. Comput. Simul. **55**, 585 (2001).
[12] B. I. Cohen, K. M. Watson, and B. J. West, Phys. Fluids **19**, 345 (1976).
[13] D. Anderson, A. Bonderson, and M. Lisak, Phys. Scr. **20**, 343 (1979).
[14] P. A. E. M. Janssen and J. J. Rasmussen, Phys. Fluids **26**, 1279 (1983).
[15] Ch. Kharif and E. Pelinovsky, Eur. J. Mech. B, Fluids **22**, 603 (2003).